The Astronomical Journal, 137:315–328, 2009 January doi:10.1088/0004-6256/137/1/315

STRATIFICATION OF METHANE ICE ON ERIS' SURFACE*

F. Merlin[1], A. Alvarez-Candal[1], A. Delsanti[1], S. Fornasier[1], M. A. Barucci[1], F. E. DeMeo[1], C. de Bergh[1], A. Doressoundiram[1], E. Quirico[2], and B. Schmitt[2]

[1] Observatoire de Paris-Laboratoire d' Études Spatiales et d' Instrumentation en Astrophysique. 5, Place Jules Janssen 92195 Meudon Cedex, France; frederic.merlin@obspm.fr

[2] Laboratoire de Planetologie de Grenoble, Bâtiment D de Physique, Domaine Universitaire B.P. 53 38041 Grenoble Cedex 9, France

Received 2008 May 6; accepted 2008 October 20; published 2008 December 15

ABSTRACT

We present new photometric and spectroscopic data of the dwarf planet Eris obtained on 2006 October and 2007 December with the Very Large Telescopes at ESO, Chile. We use three different instruments (FORS, ISAAC, and SINFONI) covering the 0.4–2.4 μm wavelength range. We show that N_2 ice is not directly detected, but the wavelength positions of the bands of CH_4 measured on the complete wavelength range seem to indicate that, as already suggested by Brown et al. and Licandro et al., a part of CH_4 ice is diluted in N_2. Spectral modeling using the Hapke theory reveals that a segregation of small and large particles of methane ice could exist on the surface. The presence of water ice and nitrogen is not completely excluded even if the respective absorption bands of these ices have not been directly detected. We present in this paper our methods to determine the wavelength shifts of the methane bands and the chemical composition from spectral modeling.

Key words: Kuiper Belt – minor planets, asteroids

1. INTRODUCTION

Eris was discovered by Brown et al. (2005) and was reported as the fourth brightest Trans-Neptunian object (TNO) after Pluto, 2005 FY_9, and 2003 EL_{61}, and the largest dwarf planet. Eris is currently close to its aphelion (≈98 AU) and is the farthest among these objects, with a heliocentric distance close to 96 AU compared with 35–51 AU for the other three largest. Eris has a highly inclined orbit (44°) whose dynamical characteristics follow that of a "detached TNO" (Delsanti & Jewitt 2006; Gladman et al. 2008) whereas the other objects are closer scattered objects or resonant objects like Pluto, trapped in a 3:2 resonance with Neptune. Bertoldi et al. (2006) derived a diameter of 3000 ± 300 km from visible and millimeter observations while Brown et al. (2006b) find a diameter of 2400 ± 100 km from a direct measurement with the *Hubble Space Telescope* (*HST*). These independent observations confirm that Eris is the largest TNO currently known, with a diameter 5%–10% larger than Pluto. Brown et al. (2006a) also discovered a satellite that has a fractional brightness of 1.9 ± 0.5% of Eris. This companion orbits 36,000 km from the primary (0.″53).

Since its discovery, this object was observed several times with different techniques. Small brightness amplitudes of the light curve in the visible have been reported by Carraro et al. (2006), Sheppard (2007), Lin et al. (2007), and Duffard et al. (2008). These observations suggest that the composition of Eris is homogeneous over the surface even if a long rotational period or a nearly pole-on view are not excluded. The phase curves and polarimetric measurements of this object have been carried out by Rabinowitz et al. (2007) and Belskaya et al. (2008), respectively. These authors show the similarities of their results with other bright objects, like Pluto or Triton: they confirm the high albedo of this object. This probably implies that Eris could be covered by freshly coated ice, as in the case of Pluto where the surface is resurfaced when it approaches perihelion (Brown et al. 2005). This assumption is well supported by the surface evolution foreseen by Schaller & Brown (2007) based on volatile loss and retention on Kuiper belt objects. In this model, volatile species such as CH_4 and N_2 can be retained by the biggest objects (Eris, Triton, and Pluto, for example), and the vaporization and sublimation of these volatiles species depend on the heliocentric distance.

These assumptions can be tested by spectroscopic observations and some information on the chemical properties of Eris have already been obtained (Brown et al. 2005; Licandro et al. 2006; Dumas et al. 2007). In fact, from these observations, Eris appears to be covered by large quantities of methane (at least 60% of the surface); other ices in smaller amounts and small amounts of organic and dark compounds are also suspected. These observations confirm the presence of the volatile CH_4 species but the status of the presence of N_2 is not clear. From the near-infrared (near-IR) observations, it is not possible to firmly detect the 2.15 μm absorption band of this component. This may be due to the low temperature that forms N_2 ice in the α-phase (undetectable with the instruments) contrary to the N_2 (in the β-phase) observed on Triton or Pluto (the transition between the α- and β-phases occurs near 35.6K). However, the visible measurements show clear wavelength shifts of the deeper methane ice band (Licandro et al. 2006) compared with those of pure methane ice, and possible wavelength shifts in the near-IR range according to different authors (Brown et al. 2005; Dumas et al. 2007; Brown 2008). Wavelength shifts have been detected in the laboratory when the methane was diluted in nitrogen matrix (Quirico & Schmitt 1997). Even if the shifts are smaller than those expected for a surface covered by methane ice in nitrogen, this suggests that a certain amount of methane diluted in nitrogen matrix may be present on the surface of Eris. Licandro et al. (2006) also show that the weakest band at 0.73 μm is almost not shifted and conclude that the diluted methane ice in nitrogen is present in the outer layer, while deeper the methane is almost pure. The goal of this paper is to compare our new observations to previous ones and to clarify the physical and chemical properties of the biggest TNO's surface.

In the first section, we present photometric and spectroscopic data, obtained with FORS1 in the visible (0.4–1 μm), and

* These observations are part of the large programme 178.C-0036.

Table 1
Observational Circumstances for Eris

Date	Instrument[a]	r[b] (AU)	δ[c] (AU)	α[d] (deg)
2006 Oct 20	F–I–S	96.849	95.890	0.16
2007 Sep 19	F–I	96.803	95.923	0.29
2007 Jul 12	I–S	96.792	96.226	0.47

Notes.
[a] Instruments (F = FORS1, I = ISAAC, S = SINFONI).
[b] Heliocentric distance.
[c] Geocentric distance.
[d] Phase angle in degrees.

ISAAC and SINFONI in the near-IR range (1.05–2.4 μm). These observations are part of the large programme 178.C-0036 dedicated to observe TNOs and Centaurs with different techniques. In the second section, we compare the obtained results to the previous ones. In the third section, we present our spectral modeling revealing the large abundances of methane on the surface of Eris and the possible presence of water ice, nitrogen ice, dark and red components (organic material and amorphous carbon, for instance). In the fourth section, we show that part of the methane absorption bands are shifted compared to the laboratory data of pure methane ice and discuss possible sources of wavelength shifts. In the last section, we discuss the results on the chemical properties of Eris and on the physical state of the CH_4 molecule before comparing them to those of Pluto and Triton.

2. OBSERVATIONS AND DATA REDUCTION

The observations of the TNO 136199 Eris presented here were obtained with the VLT (Very Large Telescope) at ESO (Chile). Near-IR photometry and spectroscopy were carried out on 2006 October 20 in service mode and on 2007 September 19 and December 7 in visitor mode with ISAAC (http://www.eso.org/instruments/isaac), installed on UT1 and SINFONI (http://www.eso.org/instruments/sinfoni), installed on UT4. We also carried out visible spectroscopy and photometry on 2006 October 20 in service mode and on 2007 September 19 in visitor mode with FORS1 (http://www.eso.org/instruments/fors1), installed on UT2. The spectra obtained in the visible are presented by Alvarez-Candal et al. (2008). Table 1 lists the details of the observational circumstances.

2.1. Photometry

Visible and near-IR observations were carried out under good photometric conditions with FORS1 and ISAAC, respectively. Photometric V, I, J, H, and K measurements (centered at 0.554, 0.768, 1.25, 1.65, and 2.16 μm, respectively) were carried out within one day, at maximum, therefore close to the spectroscopic measurements. For the near-IR observations, we used jitter imaging technique, generating a combined image with the jitter routine from the ECLIPSE package. The calibration was performed by observing several faint standard stars from Hunt et al. (1998) and Persson et al. (1998). The data reduction was performed using MIDAS and IRAF packages, and the data processing method follows that described in Romon et al. (2001). The instrumental magnitudes were measured using aperture photometry with an integrating radius typically about 3 times the average seeing. The photometric results are given in Table 2. The photometric data of 2006 October and 2007 September have been reported in DeMeo et al. (2008). The photometric values were transformed into reflectivity using solar color indices $V - J = 1.07$, $J - H = 0.29$, and $H - K = 0.06$ (Hartmann et al. 1982).

Table 3
Spectroscopic Observations of the Object

Date	UT[a]	R[b]	ET[c]	Airmass	Analog Star (Airmass)
2006 Oct 20	5:07	V	30 minutes	1.09	Landolt 93101 (1.22)
2006 Oct 20	5:12	J	40 minutes	1.10	Landolt 93101 (1.17)
2006 Oct 21	3:50	H+K	1 hr 40 minutes	1.07	Landolt 93101 (1.11)
2007 Sep 19	5:33	V	50 minutes	1.25	Landolt 93101 (1.18)
2007 Jul 12	1:10	J	36 minutes	1.07	HD2966 (1.17)
2007 Jul 12	1:00	H+K	1 hr 40 minutes	1.06	HD1368 (1.11)

Notes.
[a] Universal time at start exposure.
[b] Spectroscopic range.
[c] Exposure time.

2.2. Spectroscopy

ISAAC data: we use ISAAC not only for near-IR photometry but also to cover the J spectroscopic region from 1.1 to 1.4 μm. We use the SW mode of the instrument with a 1″ slit giving a spectral resolution of about 500. The observations were done by nodding the object along the slit by 10″ between two positions named A and B. Each pair of A and B images was combined using the MIDAS software package following the procedures described by Barucci et al. (2002). The wavelength calibration was performed using xenon and argon lamp spectral lines. The reflectivity of the object was obtained by dividing its spectrum by that of the solar analog star Landolt 93-101 or HD1368, observed at similar airmass. All the observational details are reported in Table 3.

SINFONI data: we used the SINFONI instrument to collect H- and K-band spectra of the TNO. We used the H+K spectral grating allowing us to cover H and K bands simultaneously with a spectral resolution of about 1500 and a plate scale of 250 mas pixel^{-1}. We combined several images of 10 minutes each to create a final cube. The 2006 October data reduction is reported by Guilbert et al. (2009). For the 2007 December observation, the strategy was changed in order to obtain a better extraction of the sky. The sky subtraction was performed using an IDL program kindly provided by Rick Davies (see Davies 2007) for the K band, while we used the new version of GASGANO 2.2.7 in the H band. The spectra were extracted from the individual data using QFitsView, the three-dimensional visualization

Table 2
Photometric Results Obtained

Date	$V \pm \sigma V$	$I \pm \sigma I$	$J \pm \sigma J$	$H \pm \sigma H$	$Ks \pm \sigma Ks$
2006 Oct 20	18.74 ± 0.02	18.00 ± 0.02			
2007 Sep 19	18.74 ± 0.04	18.01 ± 0.05	17.96 ± 0.07	17.88 ± 0.05	18.16 ± 0.07
2007 Jul 12			17.90 ± 0.06	17.85 ± 0.05	18.15 ± 0.06

tool developed at the Max Planck Institut für Extraterrestrishe Physik for SINFONI (http://www.mpe.mpg.de/ott/DFitsView). The individual spectra were then corrected from the remaining bad pixels and divided by the solar analog spectra. The wavelength calibration was performed using xenon, argon, and krypton lamps. In order to check the accuracy of our solar response and telluric absorption features correction, we used several solar analogs during the second night. Depending on the airmass, we measure a slight error in the slope (less than 0.5%/100 nm in H band and K band). In the case of the first night (in 2006 October) where we had only one star, we compared this star spectrum with those of the second night (in 2007 December), having a similar airmass. The 1.47–1.8 μm and 1.95–2.38 μm ranges are in good agreement between the two nights, with similar slopes (less than 1%/100 nm in H and K parts).

3. REFLECTANCE SPECTRA CONVERSION

In this section, we present our methods to obtain the final reflectance spectra of Eris in 2006 and 2007 from the spectra and the relative photometry in V, J, H, and K parts. As we need a high confidence level of the wavelength calibration to measure the position of the absorption bands with high accuracy (several angstroms), we first present the results of the wavelength calibration check. We will also explain how we normalize and adjust the different parts of the spectra to obtain complete reflectance spectra from the visible to the near-IR.

3.1. Wavelength Calibration Check

Even if the wavelength calibration is accurate using arc lines of several lamps, we need to test the wavelength calibration. In the V band, we used Franhaufer lines between 0.4 and 0.75 μm and in the near-IR, we used telluric lines of CO_2 (Goldberg et al. 1948) and stellar lines from Lançon & Rocca-Volmerange (1992) and Wallace et al. (2000). We checked that shifts are usually small, especially in the V and J parts, showing that the wavelength calibration is good with the FORS1 and ISAAC instruments (less than 1 pixel), while the errors are just a bit larger in the case of SINFONI, where the errors go up to 0.0005 μm (1 pixel). The accuracy of the wavelength calibration is around 0.0004 $\pm$ 0.0001 μm on the entire 0.4–2.45 μm wavelength range.

3.2. Reflectance Spectra

First, we need to normalize the different parts of the spectra around the wavelength corresponding to the broadband filters used for photometry (e.g., on V for the visible spectra and on J, H, and K photometric points for the near-IR spectra). We used the response curve of the FORS and ISAAC photometric filters and convolved it to our spectra over the entire wavelength range. We apply the following relation to do it:

$$V(\lambda) = [\Sigma_\lambda (R(\lambda) \cdot O(\lambda))/\Sigma_\lambda R(\lambda)] \cdot O(\lambda) \quad (1)$$

where $V(\lambda)$ is the new value for each wavelength λ of the normalized spectrum, $R(\lambda)$ is the filter response at the wavelength λ, and $O(\lambda)$ is the raw spectrum (object spectra divided by the solar analog spectrum) not normalized. In this relation, the value in between brackets is the conversion factor to transform the raw spectra. Once the normalized spectra are obtained, we multiply each spectrum by the reflectances determined by the photometry in each corresponding filter to adjust the different parts of the final spectra, from the visible to the near-IR range.

If we compare the H and K reflectance values measured in this paper with the convolution of the H and K filter responses of ISAAC with SINFONI spectra, we see small differences. If we convolve the response filter of ISAAC with our SINFONI spectra, we can compute the H/K flux ratio and compare it to the reflectances ratio H/K determined by photometry with ISAAC. We note differences of 2% in the case of the spectra of 2006 October and 1% in the case of the spectra of December 2007, showing that our results are self-consistent.

3.3. Spectral Filtering

To remove part of the data noise, we decided to replace the "bad" pixels. Bad pixels are defined using a distribution of the points around the median values. Median values are measured from the closest neighbors at each wavelength. The number of neighbors is determined by the chosen box size. In our case, we use a box of 5 pixels, corresponding to 0.0025 μm for SINFONI data, 0.0015 μm for ISAAC data, and 0.0021 μm for FORS data, which allows us to filter well and conserve the behavior of the finest absorption bands we want to detect. From this distribution, we are able to fit the Gaussian distribution and replace the data exceeding 2σ by the median value of the 5 pixel box.

The second spectrum taken in the visible range is altered by fringes, especially beyond 0.65 μm. It is difficult to remove these fringes because their frequency and amplitude are not wavelength dependent. To remove part of the fringes, at a first order, we use the spectra of the same solar analog recorded in 2006 October and 2007 September. The airmasses are slightly different but the continuums of both spectra are close. The use of this same source allows us to define the fringes that appear with the new instrumental setting. We divided the fringed spectrum of Eris by the fringes defined previously and we improved the signal-to-noise ratio (S/N) by a factor of 2–3. This spectrum was compared to that obtained in 2006 October and we note that the fringes are well removed but not completely, especially after 0.8 μm. Since the fringes are not completely removed, we point out that the measurements of the wavelength position of the absorption bands will probably be biased.

4. DISCUSSION ON THE ABSORPTION BANDS AND SPECTRAL MODELING

The spectra we have obtained in 2006 and 2007 are presented in Figure 1. They show large and deep absorption bands from the visible to the near-IR. We present here the main absorption bands and the method to model the spectra.

4.1. Overview of the Absorption Bands and Spectral Behavior

The spectra obtained in 2006 and 2007 are very similar (see Figure 2). We note the deep absorption features of methane ice along the 0.7–2.45 μm wavelength range. From these different observations, we report comparable results for the absorption depths. In the near-IR, where the spectra have been obtained with the same conditions (instrumental setting, exposure time, airmass), we report differences of the absorption bands usually lower than 10%. These differences depend on the signal to noise level of the spectra that is smaller in absorption bands (less flux). Actually, the largest differences are seen in the J band and after 2.2 μm where the signal to noise level is smaller but these differences are usually small. In both cases, the absorption bands are very deep and wide, indicating that there is a large amount of methane ice on the surface and that its thickness is large. In particular, the absorption bands between 2.2 and

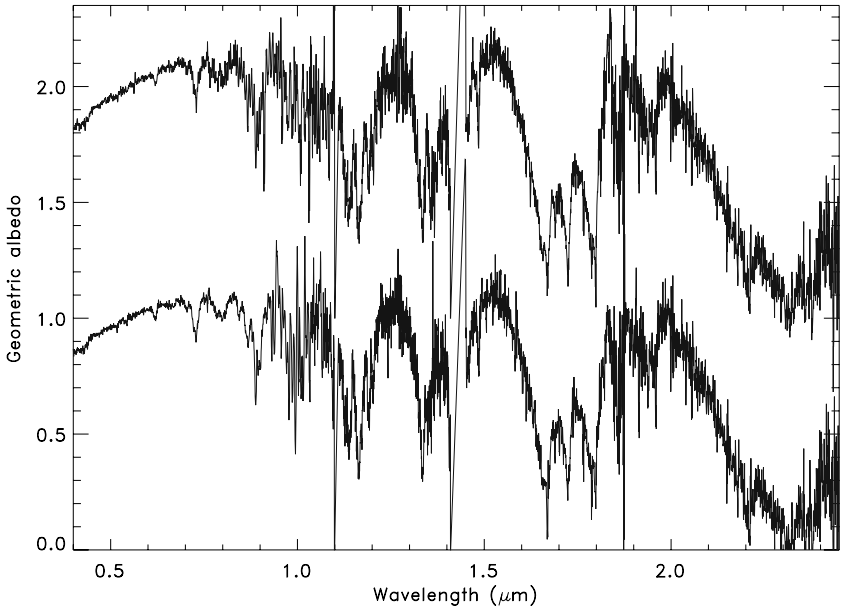

Figure 1. Entire spectra of Eris from the visible to the near-IR range. Spectra of Eris obtained in 2006 (top, shifted by +1 unity for clarity) and 2007 (bottom). We see the deep absorption bands of methane ice. We note that the 0.95–1.10, 1.35–1.48, and 1.85–1.95 μm ranges are affected by residuals in the background removal, as a part of the telluric OH lines (spikes).

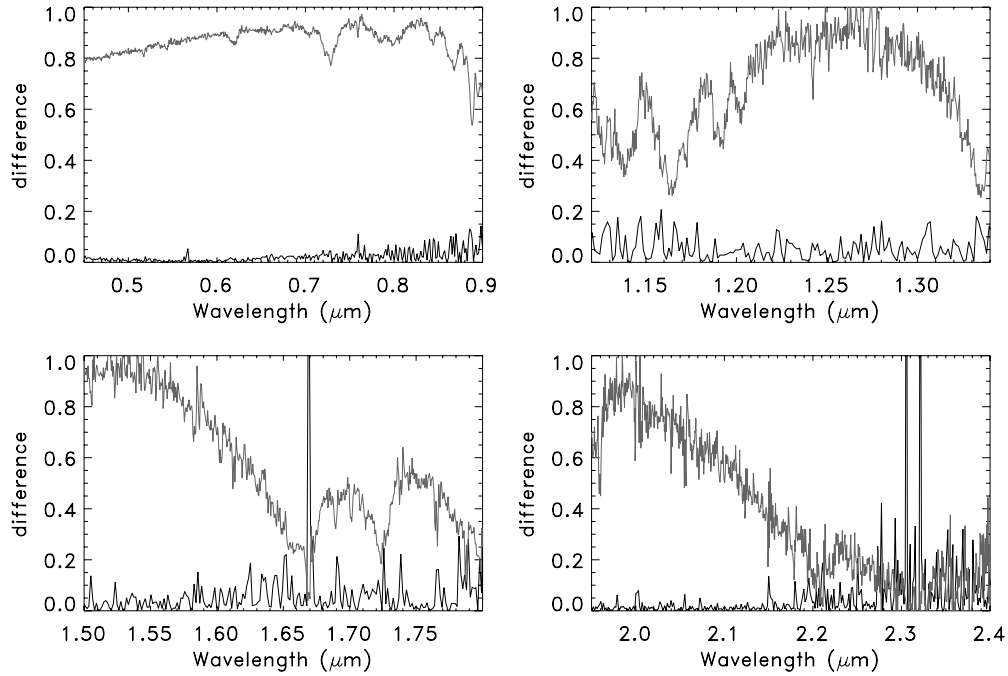

Figure 2. Reported differences between the spectra of Eris obtained in 2006 and 2007 in *V*, *J*, *H*, and *K* bands. Differences are given in % (lower curves) and shown along with the spectrum of Eris (upper curves) obtained in 2006.

2.35 μm are almost saturated. We confirm the presence of the 1.6895 μm absorption band of pure methane ice on both spectra while, ambiguous absorption features (not observed on both spectra) appear at 1.612, 1.623, 1.63, 1.695, 1.70, and 1.702 μm. These results are comparable to previous observations (Brown et al. 2005; Dumas et al. 2007) and seem to argue for a homogeneous surface, as reported from long-term photometric measurements (Sheppard 2007). In order to investigate the possibility of a homogeneous surface in detail, we ran the same comparison between the spectrum obtained in 2007 and those of Dumas et al. (2007) that include a spectrum recorded with the VLT-SINFONI instrument two years earlier (2005). The results are presented in Figure 3 and show larger differences than previously, but usually lower than 10% when the signal to noise level is high. We also computed the slope between 0.59 and 0.82 μm that is close to 4%/100 nm determined by Licandro et al. (2006). Indeed, slopes derived from our spectra give 2.4 $\pm$ 0.6% and 3.7 $\pm$ 1% for the spectra of 2006 and 2007, respectively, and 4.4 $\pm$ 2% for those of Dumas et al. (2007). These comparisons seem to confirm the homogeneous nature of Eris, already suspected from photometry.

4.2. Parameters and Limits of the Spectral Modeling

To better investigate the surface properties of this object, we ran a radiative transfer model, based on the Hapke theory that is completely described in Hapke (1981, 1993). As the phase

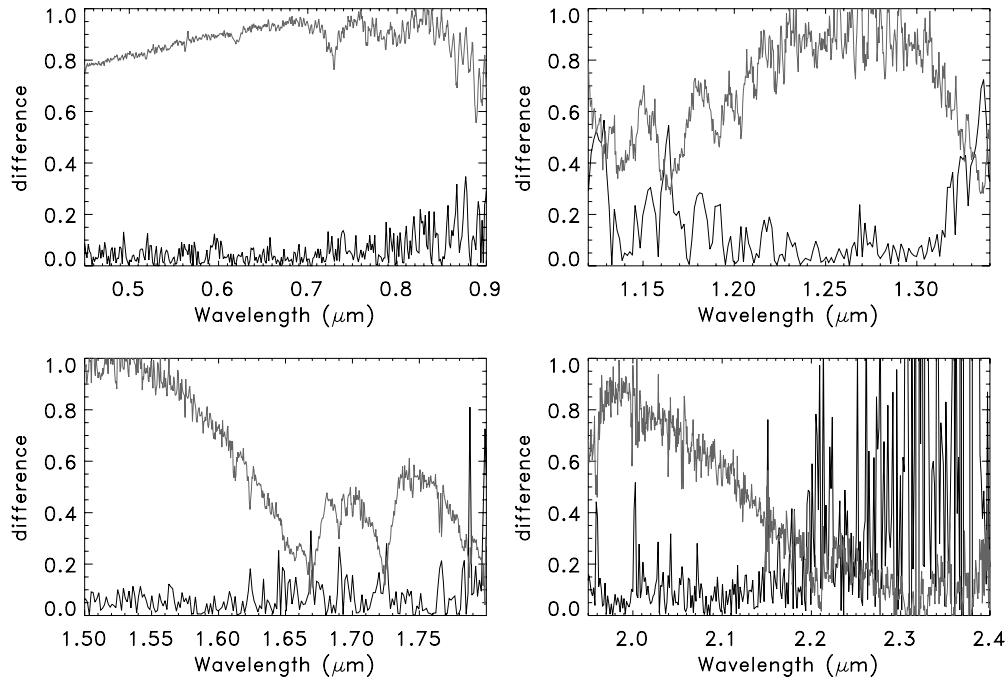

Figure 3. Reported differences between the spectra of Eris obtained in 2007 and by Dumas et al. (2007) in *V*, *J*, *H*, and *K* bands. Differences are given in % (lower curves) and shown along with the spectrum of Eris (grey curves) obtained in 2007.

angles of Eris are very small and close to 0, we compute the geometric albedo at zero phase angle from Equation (44) of Hapke (1981). In our model, a compound size and quantity are the free parameters and we use a Marqvardt–Levenberg algorithm to generate the best-fit model. This method allows us to adjust the free parameters by computing the lower χ^2 value. Our fit models are not unique but give us the most probable results from the given constraints. The given constraints are the albedo, the optical constants of different compounds, the asymmetry parameter, and the back-scattering parameter. We choose respectively an asymmetry parameter $\xi = -0.5$ and a back-scattering parameter $B_0 = 0.67$. These values are close to those of Verbiscer & Helfenstein (1998) who report the obtained values for the bigger icy satellites of the solar system. We choose an albedo of 0.86 in *V* band, as obtained by Brown et al. (2006b).

Previous papers report the presence of different ices as methane ice (Brown et al. 2006a; Dumas et al. 2007; Licandro et al. 2006), nitrogen, or water ice (Licandro et al. 2006; Dumas et al. 2007). Methane ice seems to be pure (relative to the absorption feature at 1.6895 μm) and diluted (Licandro et al. 2006). From these results, we used optical constants of pure methane ice at 40 K and isolated methane ice in nitrogen ice at 35 K (lowest temperature we have) from Quirico & Schmitt (1997). We used optical constants of crystalline water ice (Grundy & Schmitt 1998) at 40 K and those of nitrogen ice in the α-phase from Quirico et al. (1996) at 35 K. Finally, we used optical constants of organic and dark compounds. Indeed, TNOs are known to be the reddest and darkest objects of the solar system. Reddening and darkening are generated by irradiation processes (Strazzulla et al. 1991; Brunetto et al. 2006, for instance,). To reproduce these effects, we use Triton Tholin and Titan Tholin from Khare et al. (1984, 1993), which is produced from the irradiation of N_2–CH_4 mixtures and those of black carbon from Zubko et al. (1996). However, we do not know the real nature of the irradiated products present on the surface of Eris (whose surface is bright and slightly reddened) and they probably differ from these laboratory obtained materials.

Table 4
Results of the Spectral Modeling in the Different Wavelength Ranges

Wavelength Range	One Particle Size	Two Particle Sizes
0.65–1.00 μm	5.5 mm	2.0 mm + 7 cm (9:1)
		2.0 mm + 7 cm (9:1)
1.10–1.40 μm	3.5 mm	20.0 mm + 0.8 mm (35:65)
		38.0 mm + 0.9 mm (40:60)
1.45–1.85 μm	2.0 mm	8.0 mm + 0.3 mm (45:55)
		11.0 mm + 0.4 mm (45:55)
1.90–2.40 μm	2.5 mm	11.0 mm + 0.5 mm (45:55)
		13.0 mm + 0.5 mm (50:50)

Notes. Particle size and amount of methane ice obtained from spectral modeling in each wavelength range for the observations performed in 2006. In the case of the two particle sizes modeling, we have the results considering intimate mixture and geographical mixture (lines written in italic).

4.3. Results

From our spectral modeling using methane ice only, or intimate mixtures, we confirm the presence of big particles (several millimeters) of methane ice on the surface of this object.

From the models using one particle size, we can adjust only a few bands of methane ice in the different wavelength ranges (for instance, in Figures 4 and 5 for the *V* and *H* parts). Moreover, the best fits obtained with these models give different results; while a grain size exceeding 5 mm is requested in the visible range, this size drops around 2 mm in the *K* band (see Table 4). The methane properties therefore seem to change with depth (we do not probe the same layer depth at these different wavelength ranges). This trend is confirmed when two different grain sizes of methane ice are used instead of a single particle size (see Table 4). In this case, the models can fit more bands (see illustration in Figures 4

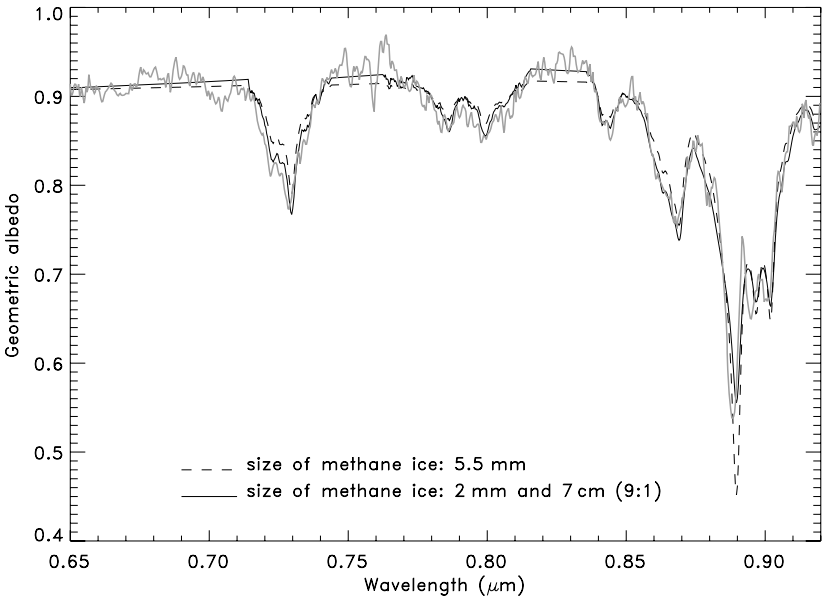

Figure 4. Spectrum of Eris in the visible and synthetic spectra. *V* spectrum of Eris (grey curves) obtained in 2006 and the best-fit Hapke model obtained with one particle size (dashed black line) and two particle sizes of methane ice using an intimate mixture (solid black line).

Table 5
Results of the Spectral Modeling in the Entire Spectra of 2006 and 2007

Species (2006)	Test 1 (i)	Test 1 (g)	Test 2 (i)	Test 2 (g)	Test 3 (i)[a]	Test 3 (g)[a]
Pure CH_4	29% 23	37% 21	32% 22	36% 23	34% 20	39% 21
	42% 1.7	27% 1.4	52% 1.2	49% 0.7	61% 0.9	53% 0.8
	28% 0.3	28% 0.5	*	*	*	*
Diluted CH_4	*	*	15% 0.2	7% 6.3	*	*
N_2	*	*	*	*	4% 0.2	1% 0.1
Titan Tholin	1% 0.07	8% 0.05	1% 0.07	8% 0.03	1% 0.07	7% 0.03
Triton Tholin	**	**	**	**	**	**
Carbon	**	**	**	**	**	**
H_2O	**	**	**	**	**	**
Reduced χ^2	0.02225	0.02257	0.02241	0.02271	0.02229	0.02225
Species (2007)	Test 1 (i)	Test 1 (g)	Test 2 (i)	Test 2 (g)	Test 3 (i)[a]	Test 3 (g)[a]
Pure CH_4	35% 13	42% 13	35% 12	36% 15	41% 12	47% 12
	39% 1.5	25% 1.3	54% 0.5	43% 0.6	55% 0.7	46% 0.6
	25% 0.2	27% 0.4	*	*	*	*
Diluted CH_4	*	*	10% 10	15% 6	*	*
N_2	*	*	*	*	3% 0.15	1% 0.1
Titan Tholin	1% 0.08	6% 0.05	1% 0.04	6% 0.03	1% 0.09	6% 0.05
Triton Tholin	**	**	**	**	**	**
Carbon	**	**	**	**	**	**
H_2O	**	**	**	**	**	**
Reduced χ^2	0.03004	0.03056	0.03105	0.03066	0.03024	0.03071

Notes. This table gives the results (amount and grain size) obtained for the different tests using intimate (i) or geographical (g) mixture models. Grain sizes are given in millimeter.
[a] The absorption band at 2.3 μm is less fitted.
* Compound not used in the model.
** Insignificant amount.

and 5). Both large and small particle grain sizes are required to fit all the absorption bands but particle sizes and relative contributions are not constant along the entire wavelength range. We obtained similar results from geographic mixtures with a small increase in the size and amount of the largest particles (see Table 4).

Finally, we ran a radiative transfer model for the two complete spectra of Eris from the visible to the near-IR. We used intimate and geographical mixtures including different grain sizes of methane ice (pure and diluted), nitrogen ice, water ice, Triton and Titan Tholins, and black carbon. Amorphous carbon and water ice are insignificant in our models. Tholins are used in small amounts, especially for intimate mixtures, and nitrogen is not mandatory. Table 5 shows the results of our modeling and Figure 6 shows the spectrum of Eris obtained in 2006 from 0.65 μm to 2.4 μm with the best-fit model which corresponds to the test 1 with intimate mixture (see Table 5 for the abundances of each compound). The grain sizes for methane ice vary from a few tenths to a few dozens millimeters.

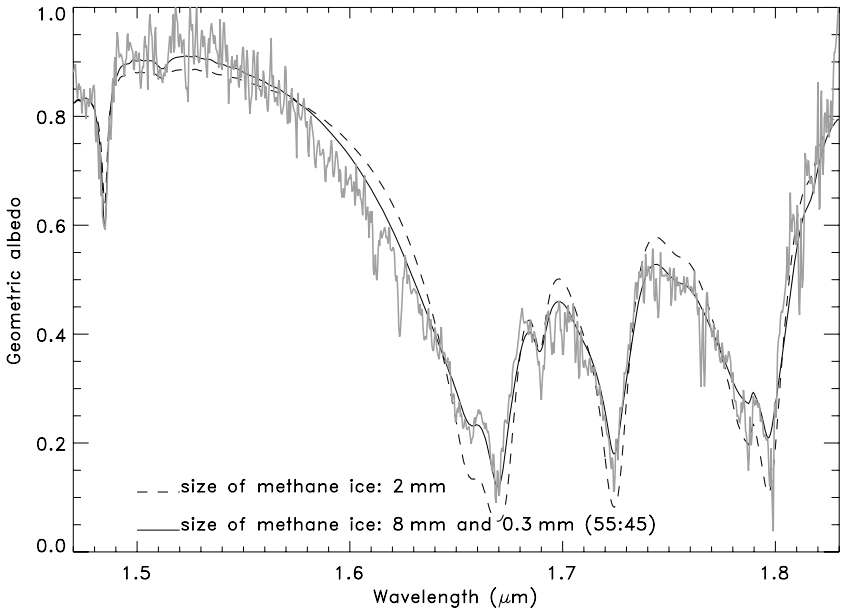

Figure 5. Spectrum of Eris in *H* band and synthetic spectra. *H* spectrum of Eris (grey curves) obtained in 2007 and the best-fit Hapke model obtained with one particle size (dashed black line) and two particle sizes of methane ice using an intimate mixture (solid black line).

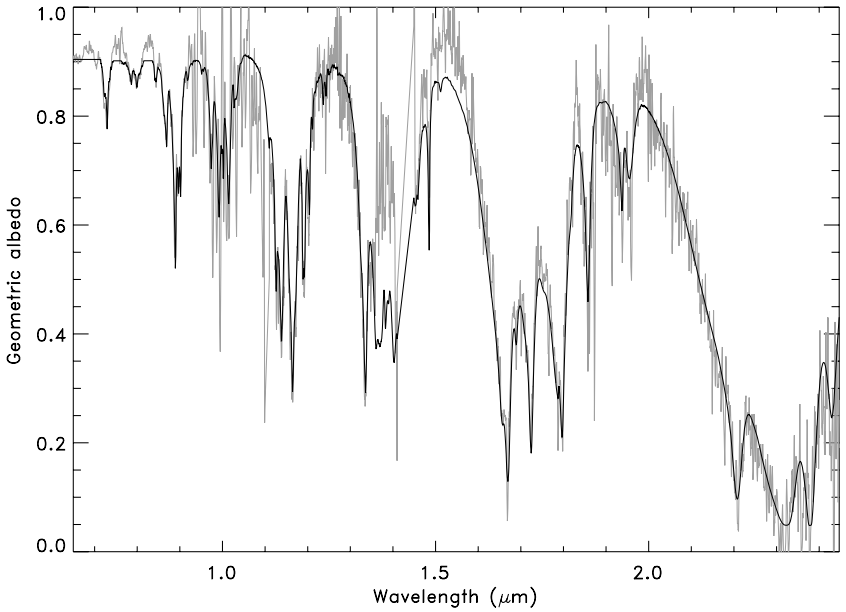

Figure 6. Spectrum of Eris from 0.65 to 2.45 μm and synthetic spectrum. Spectrum of Eris obtained in 2006 (in gray) and the best-fit model obtained from the test 1 (i) (in black; see Table 5 for details). Between 1.35 and 1.5 μm, the differences are due to bad telluric bands correction.

From Table 5, we see that from the spectral modeling, it is not possible to constrain the quantity of diluted methane ice compared to pure methane ice (similar reduced χ^2). Given the heliocentric distance of Eris, we can assume that the temperature of the surface is lower than 35.6 K and that the nitrogen ice, if present, would be in the α-phase. The use of nitrogen does not seem mandatory (similar reduced χ^2), even if it may be present, especially if it is in the α-phase where none of the absorption bands (Quirico & Schmitt 1997) could be observed with our S/N and our spectral resolution. Without a clear absorption feature, it is difficult to constrain the abundance of nitrogen ice on the surface. Furthermore, there is no need to include water ice, contrary to what was done by Dumas et al. (2007). These differences with the work of Dumas et al. (2007) are mainly due to differences in the reflectance values. Our reflectances values are greater than in the case of Dumas et al. (2007) who take the values obtained by Brown et al. (2005). Since our photometric data are consistent themselves and with those of Delsanti et al. (2008), we assume that our data are better adjusted. The amount of dark and red compounds that needs to be added seems negligible if we take into account the spectra beyond 0.65 μm but we mention that the visible part of the spectra is not well fitted. Simply, with the present database of optical constants, we cannot reproduce their effects. Without constraints on irradiated carbonaceous products, we prefer to limit our study to the 0.65–2.4 μm range. In this scope, we need optical constants of thick layers of irradiated methane ice.

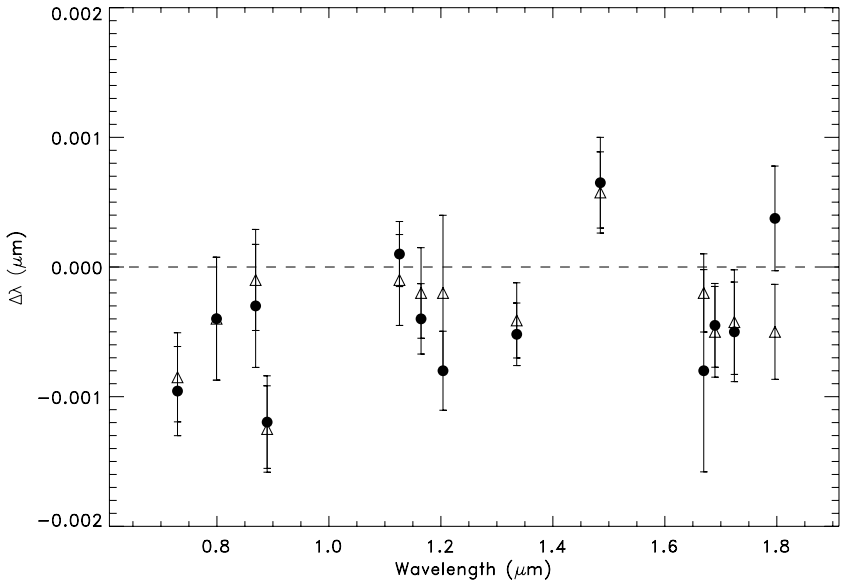

Figure 7. Results of the cross-correlation for the spectrum of 2006. Results of cross-correlation between raw (triangles) or filtered (black circles) spectra obtained in 2006 and the synthetic spectrum of pure methane ice.

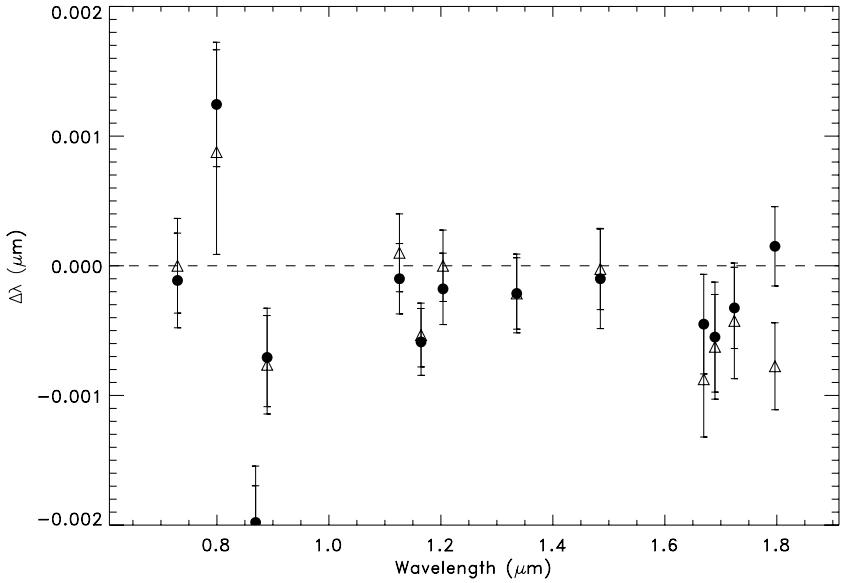

Figure 8. Results of the cross-correlation for the spectrum of 2007. Results of cross-correlation between raw (triangles) or filtered (black circles) spectra obtained in 2007 and the synthetic spectrum of pure methane ice.

5. WAVELENGTH SHIFTS

The comparison between the Eris spectra and the synthetic spectra of pure methane ice I in the pure state clearly shows differences in the peak positions of the methane absorption bands, especially in the visible range (see Figure 4). Solid methane ice presents two crystalline phases. The first one is cubic phase II, partially ordered below 20.4 K and the second one, above this temperature is cubic phase I, orientationally disordered (see Pearl et al. 1991; Hudgins et al. 1993). The methane absorption bands of Eris' spectra are blueshifted by several angstroms compared to those from synthetic spectrum of pure methane ice I. In order to quantify the shifts observed in the visible and to measure those of the near-IR, we performed a cross-correlation experiment between the entire spectra (obtained in 2006 and 2007) and the synthetic spectrum of pure methane ice I. The method is described in Tegler et al. (2008). In our case, we shift the synthetic spectra by about 30–50 Å with 3–5 Å steps (equivalent to a shift of around 11 pixels in 1 pixel steps with the different instruments). For each shift, we compute the reduced χ^2 between the shifted synthetic spectrum and the object spectrum. To derive the minimum of the reduced χ^2, we use polynomial curves that better fit the reduced χ^2 results. We derive the error of our measurements from the 2σ dispersion results obtained from the different polynomial curves (with orders from 2 to 8). For each computed shift, we estimate the total errors as the quadratic error of the experimental error and of the instrumental spectral resolution.

We note that the error bars become larger with increasing wavelength (see Figures 7 and 8). Beyond 1.8 μm, the error bars are so large that we decided to exclude these shifts from our study. The results on both spectra are quite similar in the J and H bands. We note small blueshifts (≈2–3 Å) of several

Table 6
Wavelength Shifts of the Absorption Bands (in μm) Compared to Those of Pure Methane Ice

Wavelength of Pure Methane Ice Bands*	Depth	Wavelength Shifts (2006 Spectrum)	Wavelength Shifts (2007 Spectrum)	Previous Results
0.7296 μm	18%	-0.0009 ± 0.0004	-0.0001 ± 0.0004	-0.0001 ± 0.0003[a]
0.7993 μm	07%	-0.0004 ± 0.0005	$+0.0011 \pm 0.0008$	
0.8691 μm	17%	-0.0006 ± 0.0005	-0.0020 ± 0.0004	
0.8897 μm	38%	-0.0012 ± 0.0004	-0.0008 ± 0.0004	-0.0015 ± 0.0003[a]
1.1260 μm	50%	-0.0001 ± 0.0004	-0.0000 ± 0.0003	
1.1645 μm	71%	-0.0003 ± 0.0004	-0.0005 ± 0.0002	-0.0005 ± 0.0010[b]
1.2038 μm	37%	-0.0005 ± 0.0006	-0.0001 ± 0.0003	
1.3355 μm	71%	-0.0004 ± 0.0003	-0.0002 ± 0.0003	
1.4848 μm	28%	$+0.0006 \pm 0.0003$	-0.0001 ± 0.0004	-0.0010 ± 0.0010[c]
1.6695 μm	83%	-0.0005 ± 0.0008	-0.0006 ± 0.0004	-0.0005 ± 0.0010[b]
1.6895 μm	35%	-0.0004 ± 0.0004	-0.0005 ± 0.0004	-0.0005 ± 0.0010[c]
1.7241 μm	78%	-0.0004 ± 0.0004	-0.0004 ± 0.0004	-0.0021 ± 0.0010[b]
				-0.0011 ± 0.0010[c]
1.7966 μm	72%	-0.0004 ± 0.0006	-0.0004 ± 0.0006	$+0.0004 \pm 0.0010$[c]

Notes. Wavelength shifts are the average wavelength shifts computed from the raw and filtered spectra.
* From Quirico & Schmitt (1997).
[a] From Licandro et al. (2006).
[b] From Brown et al. (2005), compared to the data of Quirico & Schmitt (1997) used in this paper.
[c] From Dumas et al. (2007).

absorption bands in this wavelength range. In the visible part, the differences between the spectra are due to the bad fringing correction in the spectrum of 2007 September. This shows us that the fringes corrected from the analog star spectrum are not the same on the object spectrum. Also, we are not able to know the error in wavelength induced by these fringes. The shifts of the visible spectrum, from 2006 October (that did not suffer from fringing), are more reliable. We note clear shifts in the shortest wavelengths for the deepest and largest bands in this wavelength range, around -10 Å. For instance, the bands at 0.7296 and 0.8897 μm reported by Grundy et al. (2002) are located at 0.7288 and 0.8885 μm respectively in our spectrum. This result confirms those of Licandro et al. (2006) who reported a similar wavelength shift for one of them (the second band measured at 0.8881 μm) and confirms that, in the visible, the deeper the band, the larger the shift. We performed the cross-correlation between the normalized raw spectra (represented by triangles in Figures 7 and 8) and the filtered spectra (represented by black circles). In both cases, the results, reported in Table 6, are usually the same revealing the accuracy of our spectral filtering. Our results are quite similar with previous results within the error bars, see Table 6, except for a few bands in the near-IR. However in this later case, the error bars are large and more accuracy would be required to make a significant comparison.

6. SOURCES OF WAVELENGTH SHIFTS

Until now, we saw wavelength shifts compared to pure methane ice I for only a few of the bands. In this section, we discuss the main possible sources of wavelength shifts.

6.1. Geographical and Intimate Icy Mixtures

To investigate whether the wavelength shifts can be induced by our spectral modeling, we measure the wavelength shifts using a cross-correlation method between pure methane ice and different ice mixtures. In our tests, the first mixture is composed of an intimate mixture of methane ice with small and large particle sizes and the second one is the best-fit model obtained in the previous section (test 1 (i); see Table 5). The results are given in Figure 9. The error bars on the figure take into account the quadratic error due to the cross-correlation method (see the previous section) and the spectral resolution of the synthetic spectra obtained using the Hapke model. In both cases, as expected, the differences are smaller than the error bars (0.0003 μm), except for a few bands, as those at 2.37 μm that is saturated. We deduce that the wavelength shifts measured by the cross-correlation method are not dependent on the spectral modeling at wavelengths smaller than 2.0 μm.

6.2. Hydrated and Diluted Materials

Laboratory measurements of the wavelength position of absorption bands of several icy mixtures reveal significant differences compared to the sum of the individual icy contributions, as in the previous section. For instance, Bernstein et al. (2005) show that the near-IR spectra of solid CO_2, in H_2O and CH_3OH are significantly different from that of pure solid CO_2. First, new absorption bands appear as forbidden bands that become deep. The second effect displays shifts in position and increasing width of the absorption bands because of intermolecular interaction with the other species (H_2O or CH_3OH). The same results have been obtained on H_2O–NH_3 mixtures by Moore et al. (2007). The authors measured near-IR and infrared spectra of pure ammonia and different hydrated ammonia at different temperatures. They show that the hydration level of ammonia plays a major role in the wavelength shifts of the reported bands. In both cases, the shifts of the bands could be very important in the near-IR, up to 0.01 μm for the CO_2 diluted in CH_3OH and 0.03 μm for hydrated ammonia. Bernstein et al. (2006) show wavelength shifts of the methane absorption bands diluted in water ice, especially when the water ice is predominant. At low temperatures, these authors measured wavelength shifts of about 0.0005–0.0010 μm for $H_2O/CH_4 = 3$. In our case, the H_2O/CH_4 is much lower than 0.1 and we estimate that the wavelength shifts, due to the dilution of CH_4 in H_2O, are negligible. Quirico & Schmitt (1997) performed laboratory measurements on simple hydrocarbons and carbon oxides diluted in solid N_2. They measured large wavelength shifts for all the absorption bands of methane and ethane ices (0.025–0.05 μm) when these ices are

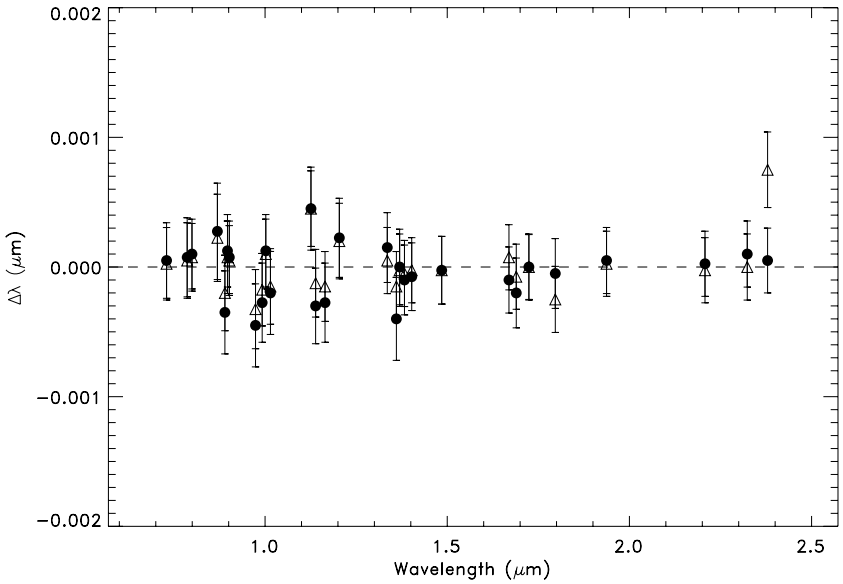

Figure 9. Cross-correlation comparing different icy mixtures. Wavelength shifts of two mixtures compared to pure methane ice. The black dots show the wavelength differences ($\Delta\lambda$) of the major absorption bands (from 0.7 to 2.5 μm) between pure methane ice (500 μm particle size) and a model made of two units consisting of a mixture of two methane ice particles with different sizes (half with a particle size of 50 μm and half with a particle size of 500 μm). The white triangles show the wavelength differences between pure methane ice (500 μm particle size) and our best-fit model for Eris.

isolated or diluted in nitrogen. The intensity of the wavelength shifts seem to be correlated with the quantity of diluted component. The higher the concentration of hydrocarbons is, the less the wavelengths are shifted. From our spectral modeling, methane ice seems to be the major component of the surface compared to nitrogen ice that seems to be less important. This implies that the wavelength shifts due to dilution are probably measurable on our spectra but that they will not be as important as observed in the laboratory work quoted above.

6.3. Temperature and Physical State

Grundy et al. (2002) reported the temperature-dependent spectrum of pure methane ice I between 0.7 and 5 μm. They measured the wavelength of the major absorption bands for temperatures between 20 and 90 K. The authors reveal different behaviors for the 61 absorption bands detected. Indeed, most of the absorption bands are sensitive to temperature, especially in the near-IR where the wavelength shifts are usually greater than 0.0005 μm between 30 and 90 K, contrary to the visible part where the shifts are in general lower. In our case, where the surface temperature of Eris is expected to be close to 20 K using the Stefan–Boltzmann law, the wavelength shifts, compared to the optical constants used in our model that correspond to a temperature of 40 K, must be very small in the visible (less than 0.00012 μm), and increase up to 0.0005 μm in the near-IR (except for a few cases, see the black circles in Figure 10). The wavelength shifts due to the temperature dependence cannot therefore be measured with our spectral resolution.

For a given species, center band positions may depend on the physical state of the ices. In the case of water ice, for instance, the absorption band near 2.00 μm is shifted if we compare amorphous and crystalline ice (Grundy & Schmitt 1998). For ammonia, Moore et al. (2007), report important wavelength shifts between amorphous and cubic states. The physical state of the components is linked with the equilibrium temperature. From Figure 10, we see that important wavelength shifts can be due to state differences. The triangles in the figure show differences between the phase II at 20 K (Grundy et al. 2002) compared to the phase 1 at 40 K. As mentioned previously, the temperature of Eris is close to 20 K, 15 K for an albedo of 0.93 (upper limit found by Brown et al. 2005), and 24 K for an albedo of 0.50 (lowest limit found by Bertoldi et al. 2006). So, it is possible that the methane is in phase II. In this case, blueshifts observed in the visible could be due to the physical state of methane ice (shifts of 0.0008 μm for the absorption bands close to 0.9 μm).

6.4. Irradiation Effects

Numerous authors have studied the effects of irradiation on icy bodies. The major effects are a decrease in albedo and reddening of the surface. Other phenomena are also observed. In the case of water ice, the absorption band feature of the crystalline state, located near 1.65 μm, can change with irradiation. Irradiation modifies the crystalline water ice in an amorphous state (e.g., Strazzulla et al. 1991; Moore & Hudson 1992; Mastrapa & Brown 2006). This phenomenon is also observed in the case of ion-irradiated frozen methanol (Brunetto et al. 2005) where the shape at 2.28 μm is shifted toward shorter wavelengths after irradiation. However, in the latter case, irradiation processes form new species and erase completely the second band of methanol at 2.33 μm, giving us an indicator of the irradiation state of this molecule. Gerakines et al. (1996), Baratta et al. (2002), Moore & Hudson (2003), and Bennett et al. (2006) have photolyzed frozen methane ice with UV photons, and irradiated it with proton and electron flux, respectively. In all the cases, a part of the initial methane was destroyed, generating other species. Ethane and ethylene are the major products in the case of electron irradiation, and Baratta et al. (2002) report high production of ethane from He+ irradiation and UV photolysis. Search for irradiated products could inform us of the irradiated state of Eris surface.

In order to constrain the quantity of irradiated materials, we ran a radiative transfer model to adjust Eris' spectrum (see Section 4 for more details). We used optical constants of the compounds used previously (see Section 5) and added alternately those of pure ethylene ice and pure ethane ice at 21 K

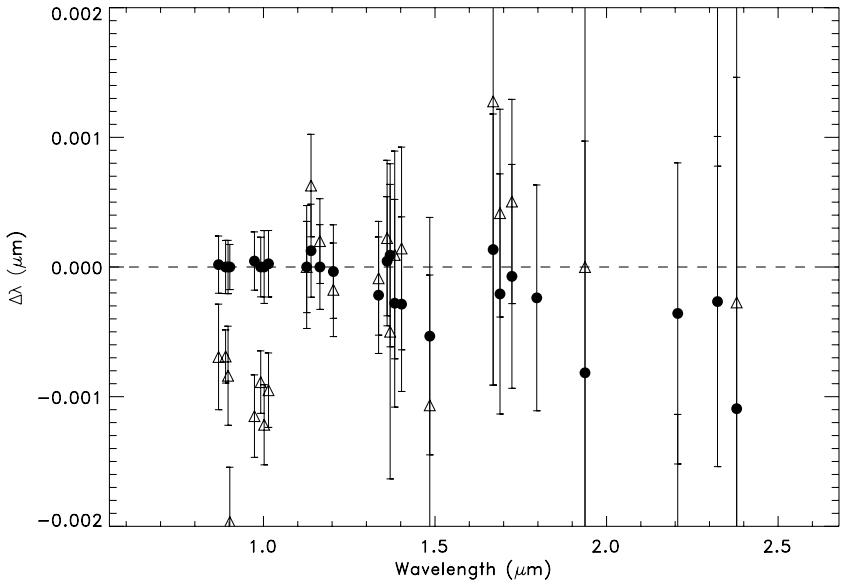

Figure 10. Cross-correlation comparing different temperatures and physical states of methane ice. Cross-correlation between synthetic spectra of methane ice at 40 K with methane ice at 30 K (black circles) and 20 K (triangles). Measurements start at 0.89 μm because laboratory data at shorter wavelengths are highly noisy.

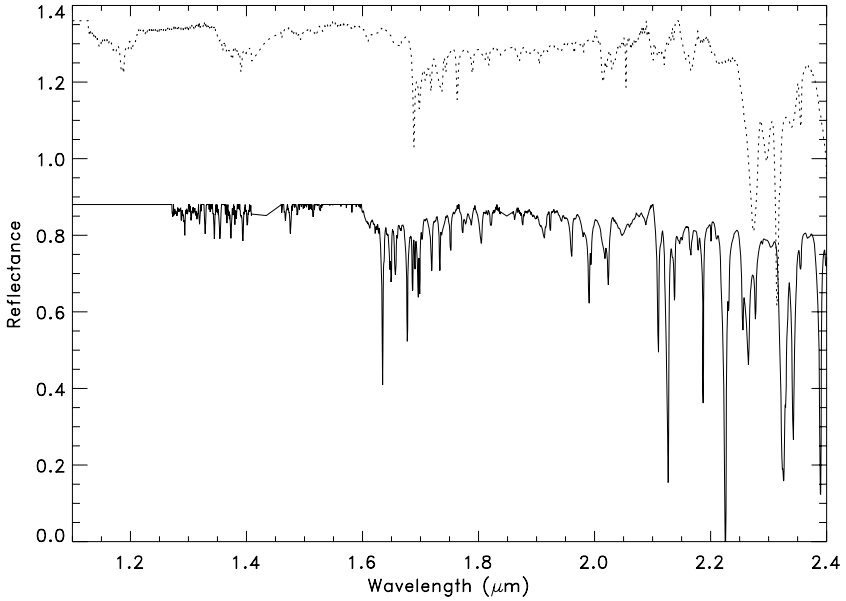

Figure 11. Reflectance spectra of ethane (dotted line) and ethylene (continuous line). The reflectance spectra were shifted of +0.4 and −0.1, respectively, for clarity. The deepest and largest bands appear between 2.0 and 2.4 μm.

(Quirico & Schmitt 1997). These optical constants allow us to compare the fit with and without these probable irradiated products. Ethane and ethylene absorption bands are deep and numerous, especially in the 1.6–2.4 μm wavelength range (see Figure 11). The use of ethylene and ethane modifies slightly the absorption features in *K* band, where the absorption bands are deeper (see Figure 12). The reduced χ^2 is slightly lower with ethane (0.0219 versus 0.02225 without ethane) and slightly larger with ethylene (0.02250). The model using ethane requires 6% of this compound (60 μm particle size), 1% of Titan Tholin, and 94% of methane ice (with three different particle sizes from 600 μm to 19 mm) while the best-fit model using ethylene requires 4% of this compound (40 μm particle size), 1% of Titan Tholin, and 95% of methane ice (with three larger particle sizes from 600 μm to 18 mm). As the quantity of the compounds depends of the particle size, we ran several spectral models using different grain sizes in order to determine the upper limit amount of these compounds. From 10 μm to 100 μm particle size, we have similar reduced χ^2 within 2%. We found a rate range between 1.7 and 3.3% in the case of ethylene, and between 4 and 6% in the case of ethane. At this step, it appears that the presence of ethane is more probable than that of ethylene, that it is consistent with laboratory measures (Bennett et al. 2006). Finally, we ran our models using rates 2 times larger (5% of ethylene and 10% of ethane). With these amounts, we note clear disagreements in the 2.1–2.3 μm wavelength range (see Figure 13). This allows us to conclude that less than 10% of ethane and less than 5% of ethylene could be present on the surface, but better signal to noise level are required to clearly identify the absorption features of these irradiated products. From Bennett et al. (2006), these quantities could be obtained from small doses of electron and proton irradiation (few eV

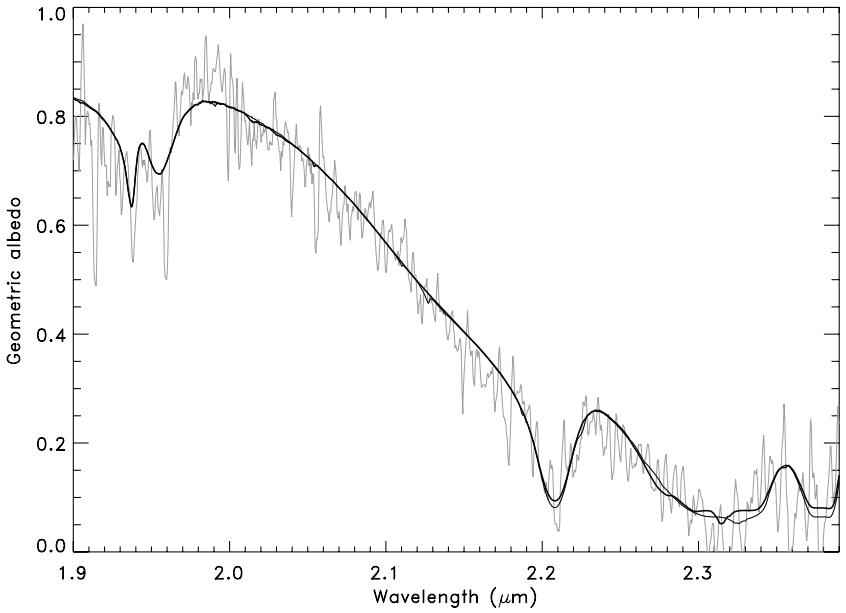

Figure 12. Spectrum of Eris (grey line) obtained in 2006 October and spectral modeling obtained with ethane (thick black line) and with ethylene (thin black line). The differences are small and appear close to 2.02, 2.06, 2.13, and 2.3 μm.

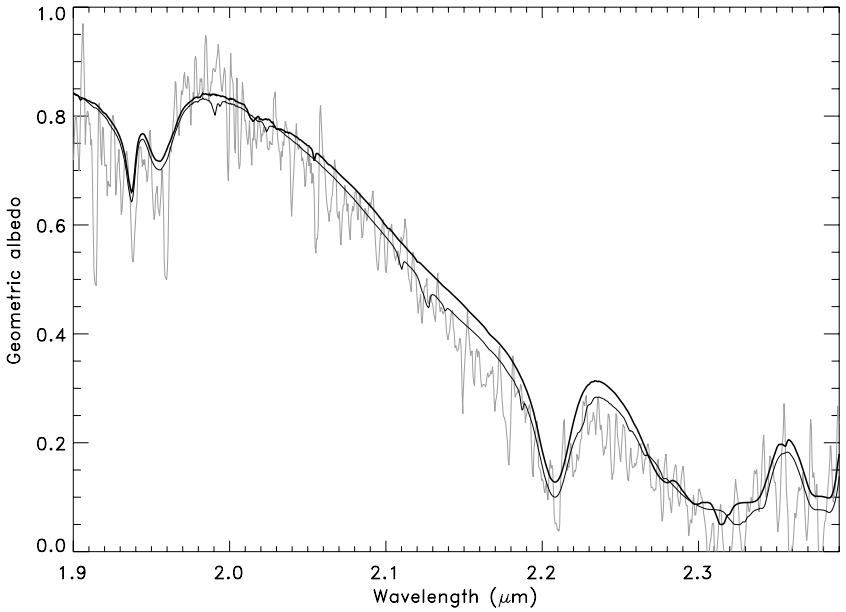

Figure 13. Spectrum of Eris (grey line) obtained in 2006 October and spectral modeling obtained with 10% of ethane (thick black line) and 5% of ethylene (thin black line). These quantities appear as the upper limits.

per molecule). However, the red slope observed in the visible seems to require larger doses from Brunetto & Roush (2008), at least a hundred eV per molecule. This tends to indicate that the simple products of irradiation are themselves destroyed to form more complex products (i.e., organics). The effects of irradiation on the wavelength positions of the methane ice bands are not yet known. Contrary to the cases of methanol or water ice, where irradiation induces hydrogen bending modification between molecules and reorganizes the main structure (from the crystalline to the amorphous state, for instance), we can assume that irradiated methane is probably entirely converted to other species and that this process has small effects on line positions.

7. DISCUSSION

From the previous discussion on the different possible sources of wavelength shifts, we conclude the following:

1. Temperature dependence is too weak for methane ice, especially close to the temperature of Eris' surface, assumed to be about 20 K.
2. The physical state of methane is not yet constrained but we cannot exclude a surface covered by methane ice in phase II.
3. Part of the methane ice is in the pure state, according to the presence of the 1.6895 μm absorption band.

4. Part of the methane ice could be diluted in N_2, inducing wavelength shifts.
5. Irradiation processes seem to have negligible effects on wavelength positions, especially compared to those of the dilution and/or change of ice state effects.

To conclude, we have two possibilities to explain these wavelength shifts. The first one is to assume that the wavelength shifts compared to pure methane ice I at 40 K are due to a different physical state (phase II). In this case, we would have blueshifts in the visible range and redshifts or nothing in the near-IR range. However, the results (see Figures 7 and 8) do not show this trend in the near-IR (we tend to have blueshifts rather than redshifts, even if the error bars are large). Another trend that argues in favor of methane ice in phase I is the behavior of the absorption bands in the *H* and *K* parts. In these spectral ranges, the absorption bands in phase II are finer than in phase I, which is not the case on the Eris spectra where we have large absorption bands. Moreover, the absorption feature at 1.657 μm is only present in the case of phase I (Grundy et al. 2002). To derive the temperature of the methane ice, Grundy et al. (2002) reported that the temperature affects not only the position of the bands but also their behaviors. Indeed, the width at half maximum of several bands is correlated with the temperature (FWHM for many of the bands is nearly proportional to temperature). However, it could be difficult to derive the temperature from the FWHM because spectral effects due to multiple scattering in complex surfaces can be quite similar to the band-broadening effects of increasing temperature. For this reason we cannot try to measure the temperature of the icy surface of Eris and constrain the methane ice phase since our spectral modeling suggests a complex surface. Even if new observations at better S/N are required to determine the phase of the methane ice, it seems more probable that this ice is in phase I and that the wavelength shifts are due to dilution.

The presence and quantity of nitrogen ice could not be determined by spectral modeling due to the lack of a clear absorption feature close to 2.15 μm. However, the wavelength shifts of the methane ice absorption bands suggest the presence of nitrogen ice. Wavelength shift depends on the relative quantity of methane ice compared to nitrogen ice. When the concentration of methane is very low, the interactions with nitrogen atoms are high and the wavelength shifts can be large. On the contrary, if the methane concentration is high, the medium tends to have pure methane ice properties with few interactions with nitrogen atoms. We therefore expect that the lack of the nitrogen feature is due to the fact that the surface temperature is lower than 35.6 K and that this ice is in the α-phase and not detectable with our spectral resolution. It is also possible that the quantity of nitrogen is not important enough to be detectable.

Quirico & Schmitt (1997) show that the intensity of the shifts also depends on the absorption bands. The shifts of the methane absorption bands diluted in nitrogen compared to those of pure methane ice are generally smaller at smaller wavelengths. Indeed, in the visible and in the near-IR, we have a combination of wavelength shifts corresponding to the combination of different modes. For instance, the absorption band at 2.3240 μm, corresponding to the ν_3+ν_4 mode, is shifted by 0.0053 μm while the absorption band at 1.1645 μm, corresponding to the $2\nu_4$+$2\nu_3$ mode, is shifted by 0.0031 μm (corresponding to 2 times larger in frequency). The last dependence of the spectral shifts is the temperature of the diluted or isolated medium. The wavelength shifts are more important at lower temperatures (Quirico & Schmitt 1997). In a few cases, the wavelength shifts are amplified when the nitrogen is in the α-phase. Without knowledge of the dilution state and of the temperature of the ice, it appears difficult to determine constraints on these physical properties. However, several modes such as $3\nu_4$ or ν_2+$2\nu_4$ are not temperature dependent in the case of isolated methane. We can therefore derive the dilution state from these modes and then, the temperature from other ones (e.g., ν_2+ν_3, ν_3+$2\nu_4$, or $2\nu_3$). Our signal to noise level and the results obtained by cross-correlation do not allow us to determine the wavelength shifts with accuracy, especially beyond 1.8 μm (lower than 5500 cm^{-1}) where the $3\nu_4$ and the ν_2+$2\nu_4$ modes are observable. New observations with a higher S/N are required to better investigate these physical properties.

From the results of the wavelength shifts, we find that the deepest bands in the visible are more shifted than the weakest, and confirm the results previously obtained by Licandro et al. (2006) who suggests a stratification of the diluted methane ice. Indeed, from the visible range, it seems that the deeper we probe the surface, the less the methane is diluted. At the same time, we saw that the wavelength shifts are of the same order or less important in the near-IR compared to the visible, while the contrary is expected for a given dilution state. This suggests that the dilution of methane ice is less important from the near-IR observations than the visible ones. This may imply a methane ice dilution stratification where we could find a diluted methane ice layer between two layers of pure methane ice. From spectral modeling, the largest particle sizes are required in the visible range, especially for the weakest bands, while the smallest particle sizes are required in the near-IR where the bands are the deepest. From these models and the results on wavelength shifts, we can therefore assume that the first millimeters probed cross pure methane ice before passing a diluted methane ice layer. A spectral modeling using stratification could be very useful to well constrain the structure of the surface.

Compared to Triton and Pluto, Eris' spectra do not show any evidence of nitrogen nor other highly volatile ices besides methane ice. The spectrum of Triton (see Quirico et al. 1999) clearly shows nitrogen, CO, and CO_2 features from 1.9 to 2.5 μm. The spectra of Pluto also show absorption features of CO and nitrogen in the near-IR (see Olkin et al. 2007; Doute et al. 1999). The presence of nitrogen in the β-phase for Pluto and Triton indicates that the surface temperature of these objects is higher than 35.6 K and that the methane ice is in phase I. Wavelength shifts observed in the near-IR by these authors revealed that methane ice is isolated in the N_2 matrix on Triton and partially isolated on Pluto (a part of the methane is pure on the surface of Pluto). Eris seems to be covered by more pure methane ice than the other two objects. Indeed, the absorption feature at 1.689 μm, which appears only for pure methane ice, is more pronounced on the Eris spectra and the wavelength shifts in the near-IR are less remarkable. The quantity of nitrogen on Eris' surface is probably smaller and less important than on the surfaces of Triton and Pluto.

8. CONCLUSION

We presented new spectra of Eris covering the 0.37–2.45 μm range. We have shown that pure methane ice I at low temperature cannot reproduce our observations. We confirm the wavelength shifts of absorption bands of methane ice (compared to pure methane ice I) and measure new ones in the visible range while the near-IR absorption bands seem not so shifted. We have shown that the most probable explanation for these wavelength

shifts is the dilution of methane ice in nitrogen, as assumed by Licandro et al. (2006). We note that a different physical state for the methane ice (the lower temperature phase II) could generate comparable effects in the visible but not completely in the near-IR. Better constrains on the surface temperature are required to conclude on this, especially in the *K* band where the spectral behavior is related to the ice temperature and around 1.45 μm where new bands appear in the case of methane ice in phase II (temperature lower than 20.4 K). Moreover, these observations suggest a stratification of the diluted methane ice, with a layer of diluted methane ice between two layers of pure methane ice. We can suggest that we have depleted nitrogen in the deepest layers after sublimation processes that enrich adjacent layers during condensation processes. The first micrometers, more irradiated, could be formed by a nitrogen-depleted layer or, perhaps, diluted methane ice is more easily destroyed than pure methane ice. Laboratory measurements would be very useful to investigate the possibilities to form this kind of stratification. The quantity of nitrogen on Eris' surface is probably smaller and less important than on the Triton's and Pluto's surfaces, as the quantity of other volatile species (CO and CO_2). New spectra with a higher signal to noise level would be very helpful to confirm these trends.

We are grateful to C. Dumas for his help on the acquisition and reduction of SINFONI data and the referee for his/her valuable comments.

REFERENCES

Alvarez-Candal, A., Fornasier, S., Barucci, M. A., de Bergh, C., & Merlin, F. 2008, A&A, 487, 741
Baratta, G. A., Leto, G., & Palumbo, M. E. 2002, A&A, 384, 343
Barucci, M. A., et al. 2002, A&A, 392, 335
Belskaya, I., Bagnulo, S., Muinonen, K., Barucci, M. A., Tozzi, G. P., Fornasier, S., & Kolokolova, L. 2008, A&A, 479, 265
Bennett, C. J., Jamieson, C. S., Osamura, Y., & Kaiser, R. I. 2006, ApJ, 653, 792
Bernstein, M. P., Cruikshank, D. P., & Sandford, S. A. 2005, Icarus, 179, 527
Bernstein, M. P., Cruikshank, D. P., & Sandford, S. A. 2006, Icarus, 181, 302
Bertoldi, F., Altenhoff, W., Weiss, A., Menten, K. M., & Thum, C. 2006, Nature, 439, 563
Brown, M. E. 2008, The Solar System Beyond Neptune, ed. M. A. Barucci, et al. (Tucson, AZ: Univ. Arizona), 335
Brown, M. E., Schaller, E. L., Roe, H. G., Rabinowitz, D. L., & Trujillo, C. A. 2006a, ApJ, 643, L61
Brown, M. E., Trujillo, C. A., & Rabinowitz, D. L. 2005, ApJ, 635, L97
Brown, M. E., et al. 2006b, ApJ, 639, L43
Brunetto, R., Baratta, G. A., Domingo, M., & Strazzulla, G. 2005, Icarus, 175, 226
Brunetto, R., Barucci, M. A., Dotto, E., & Strazzulla, G. 2006, ApJ, 644, 646
Brunetto, R., & Roush, T. L. 2008, A&A, 481, 879
Carraro, G., Maris, M., Bertin, D., & Parisi, M. G. 2006, A&A, 460, L39
Davies, R. I. 2007, MNRAS, 375, 1099
Delsanti, A., Doressoundiram, A., & Peixinho, N. 2008, LPI Contributions, 1405, 8136
Delsanti, A., & Jewitt, D. 2006, Solar System Update, ed. P. Blondel & J. Mason (Berlin: Springer), 267
DeMeo, F. E., et al. 2008, AAS/Division for Planetary Sciences Meeting Abstracts, 40, #47.05
Douté, S., Schmitt, B., Quirico, E., Owen, T. C., Cruikshank, D. P., de Bergh, C., Geballe, T. R., & Roush, T. L. 1999, Icarus, 142, 421
Duffard, R., Ortiz, J. L., Santos Sanz, P., Mora, A., Gutiérrez, P. J., Morales, N., & Guirado, D. 2008, A&A, 479, 877
Dumas, C., Merlin, F., Barucci, M. A., de Bergh, C., Hainault, O., Guilbert, A., Vernazza, P., & Doressoundiram, A. 2007, A&A, 471, 331
Gerakines, P. A., Schutte, W. A., & Ehrenfreund, P. 1996, A&A, 312, 289
Gladman, B., Marsden, B. G., & Vanlaerhoven, C. 2008, in The Solar System Beyond Neptune, ed. M. A. Barucci et al. (Tucson, AZ: University of Arizona Press), 43
Goldberg, L., Mohler, O., & McMath, R. 1948, Phys. Rev., 74, 1881
Grundy, W. M., & Schmitt, B. 1998, J. Geophys. Res., 103, 25809
Grundy, W. M., Schmitt, B., & Quirico, E. 2002, Icarus, 155, 486
Guilbert, A., et al. 2009, Icarus, submitted
Hapke, B. 1981, J. Geophys. Res., 86, 3039
Hapke, B. 1993, Topics in Remote Sensing (Cambridge: Cambridge Univ. Press)
Hartmann, W. K., Cruikshank, D. P., & Degewij, J. 1982, Icarus, 52, 377
Hudgins, D. M., Sandford, S. A., Allamandola, L. J., & Tielens, A. G. G. M. 1993, ApJS, 86, 713
Hunt, L. K., Mannucci, F., Testi, L., Migliorini, S., Stanga, R. M., Baffa, C., Lisi, F., & Vanzi, L. 1998, AJ, 115, 2594
Khare, B. N., Sagan, C., Arakawa, E. T., Suits, F., Callcott, T. A., & Williams, M. W. 1984, Icarus, 60, 127
Khare, B. N., Thompson, W. R., Cheng, L., Chyba, C., Sagan, C., Arakawa, E. T., Meisse, C., & Tuminello, P. S. 1993, Icarus, 103, 290
Lançon, A., & Rocca-Volmerange, B. 1992, A&AS, 96, 593
Licandro, J., Grundy, W. M., Pinilla Alonso, N., & Leisy, P. 2006, A&A, 458, L5
Lin, H.-W., Wu, Y.-L., & Ip, W.-H. 2007, Adv. Space Res., 40, 238
Mastrapa, R. M. E., & Brown, R. H. 2006, Icarus, 183, 207
Moore, M. H., Ferrante, R. F., Hudson, R. L., & Stone, J. N. 2007, Icarus, 190, 260
Moore, M. H., & Hudson, R. L. 1992, ApJ, 401, 353
Moore, M. H., & Hudson, R. L. 2003, Icarus, 161, 486
Olkin, C. B., et al. 2007, AJ, 133, 420
Pearl, J., Ngoh, M., Ospina, M., & Khanna, R. 1991, J. Geophys. Res., 96, 477
Persson, S. E., Murphy, D. C., Krzeminski, W., Roth, M., & Rieke, M. J. 1998, AJ, 116, 2475
Quirico, E., Doute, S., Schmitt, B., de Bergh, C., Cruikshank, D. P., Owen, T. C., Geballe, T. R., & Roush, T. L. 1999, Icarus, 139, 159
Quirico, E., & Schmitt, B. 1997, Icarus, 127, 354
Quirico, E., Schmitt, B., Bini, R., & Salvi, P. R. 1996, Planet. Space Sci., 44, 973
Rabinowitz, D. L., Schaefer, B. E., & Tourtellotte, S. W. 2007, AJ, 133, 26
Romon, J., de Bergh, C., Barucci, M. A., Doressoundiram, A., Cuby, J.-G., Le Bras, A., Douté, S., & Schmitt, B. 2001, A&A, 376, 310
Schaller, E. L., & Brown, M. E. 2007, ApJ, 659, L61
Sheppard, S. S. 2007, AJ, 134, 787
Strazzulla, G., Leto, G., Baratta, G. A., & Spinella, F. 1991, J. Geophys. Res., 96, 17547
Tegler, S. C., Grundy, W. M., Vilas, F., Romanishin, W., Cornelison, D., & Consolmagno, G. J. 2008, Icarus, 195, 844
Verbiscer, A., & Helfenstein, P. 1998, in Solar System Ices, Vol. 227, Reflectance Spectroscopy of Icy Surfaces, ed. B. Schmitt, C. de Bergh, & M. Festou (Dordrecht: Kluwer), 157
Wallace, L., Meyer, M. R., Hinkle, K., & Edwards, S. 2000, ApJ, 535, 325
Zubko, V. G., Mennella, V., Colangeli, L., & Bussoletti, E. 1996, MNRAS, 282, 1321